# High efficient Al: ZnO based bifocus metalens in visible spectrum*

Pengdi Wang(王鹏迪)[1] and Xianghua Zeng(曾祥华)[1,2,†]

[1] College of Physics Science and Technology & Institute of Optoelectronic Technology, Yangzhou University, Yangzhou 225002, China
[2] College of Electrical, Energy and Power Engineering, Yangzhou University, Yangzhou 225127, China

(Received 2 April 2020; revised manuscript received 21 June 2020; accepted manuscript online 1 August 2020)

The optical components of the visible light band are widely used in daily life and industrial development. However due to the serious loss of light and the high cost, the application is limited. The broadband gap metasurface will change this situation due to its low absorption and high efficiency. Herein, we simulate a size-adjustable metasurface of the Al doped ZnO (AZO) nanorod arrays based on finite difference time domain method (FDTD) which can realize the conversion of amplitude polarization and phase in the full visible band. The corresponding theoretical polarization conversion efficiency can reach as high as 91.48% (450 nm), 95.27% (530 nm), and 91.01% (65 nm). The modulation of focusing wavelength can be realized by directly adjusting the height of the AZO nanorod. The designed half-wave plate and metalens can be applied in the imaging power modulation halfwave conversion and enriching the spectroscopy.

**Keywords:** visible spectrum, Al doped ZnO, half-wave plate, metalens

**PACS:** 42.79.−e, 42.79.Bh **DOI:** 10.1088/1674-1056/abab70

## 1. Introduction

Visible light plays an important role in our lives. The details of the object can be observed directly under visible light using a convex lens. The traditional optical microscope uses the principle of light refraction to realize the aggregation of the light source. However, the refractive index of different wavelengths in the lens is inconsistent, resulting in the color difference of the displayed image. The common method is to correct the optical color difference by using a multi-layer lens. This method has many disadvantages, such as increasing lens thickness which goes against for installation, expensive, easy to wear, smaller numerical aperture (NA), and so on. The more suitable solutions are to eliminate chromatic aberration by improving the sensor or to construct the broadband gap semiconductor metasurface. The latter has become the main research focus due to the advantages of low cost, simple structure, and high focusing efficiency. The earliest studies[1,2] were reported in 2007, it gradually came into effect. For example, Mohammadreza *et al.*[3] reported that the metalens was capable of focussing and subwavelength imaging in the visible region. Now the metalens has attracted much attention,[4–7] and many kinds of semiconductors have been used in the development of metalens, such as GaAs,[8] AlN,[9] GaN,[10] and so on. Kelly *et al.*[11] showed that the Al doped ZnO (AZO) has the ability of hyperbolic dispersion in the infrared region, indicating the potential applications. Masouleh *et al.*[12] showed that increasing the free electron concentration of the AZO will produce a negative dielectric constant in the infrared band with a low photon loss. Based on these, Li *et al.*[13] developed a complex multilayer metalens based on the AZO that can achieve subwavelength imaging in the infrared region.

As a wide bandgap (∼3.2 eV) semiconductor, ZnO is a non-toxic and non-polluting material, which can be widely used in optical devices. The AZO materials exhibit good transparency and conductivity. And the different content Al doping in ZnO will cause many physical properties, such as changing bandwidth[14–16] and refractive index.[17] However, the metalens based on AZO nanorods of visible-light region, especially multifocal ones, have rarely been reported. Due to the low efficiency of polarity conversion and the high cost of development, it is necessary to develop a cheap and efficient metasurface, which can not only achieve efficient polarization conversion but also be used for high-speed microscopy and other optical applications.

The Pancharatnam–Berry phase (PB) phase method[18] was used to generate a broadband vortex beam by Xu *et al.*[19] It is an important way to design the metalens from simulation, as the simulated results will help us to find suitable materials with some typical structures.[20,21] Due to its good properties of transparency and conductivity, and bandgap tuning, herein we used the PB phase method to design the AZO metalens based on half-wave plates in the visible range, one-dimensional (1-D) transversal metalens with a length of 20 μm was constructed. The simulation result showed that it has a high focusing ability in a circle with a diameter of smaller than 10 μm. Then, we designed two-dimensional (2-D) metalens with a size of 8 μm×8 μm and its feasibility was confirmed by simulation. Furthermore, the designed metalens was found

*Project supported by the National Key Research and Development Program of China (Grant No. 2017YFB0403101).
†Corresponding author. E-mail: xhzeng@yzu.edu.cn
 

to have two focal points, which was not reported before. By regulating the coverage area range of meta-atoms on the surface of the metalens, the focal length and the number of focal points can be varied.

## 2. Structure design and methods

We select 2% AZO as the experimental material. In addition, to facilitate the study of the entire visible light band, we use the central wavelength of the three-primary colors as the representative of visible light, blue (435–480 nm), green (500–560 nm), and red (605–700 nm), where the values of 450 nm, 530 nm, and 650 nm are used for research objects. The structure is displayed in Figs. 1(a)–1(e). Figure 1(a) shows a single cell containing single AZO nanocolumn on the ITO substrate. The fast axis ($ox'$) is perpendicular to the slow axis $oy'$, and the rotation angle ($\theta$) of the nanorod is defined by the angle between the fast axis and the $x$ axis. And the refractive index $n$ and extinction coefficient $k$ can be obtained from the website (https://refractiveindex.info/), as shown in Fig. 1(f)).

All experiments are performed with the FDTD software developed by Lumerical Inc. The simulation region is selected with periodic boundary conditions on the $x$ and $y$ axes, and perfectly matched layers one on the $z$ axis. The simulation time is 1000 fs and the convergence criteria are set to have an auto shutoff minimum of $10^{-5}$.

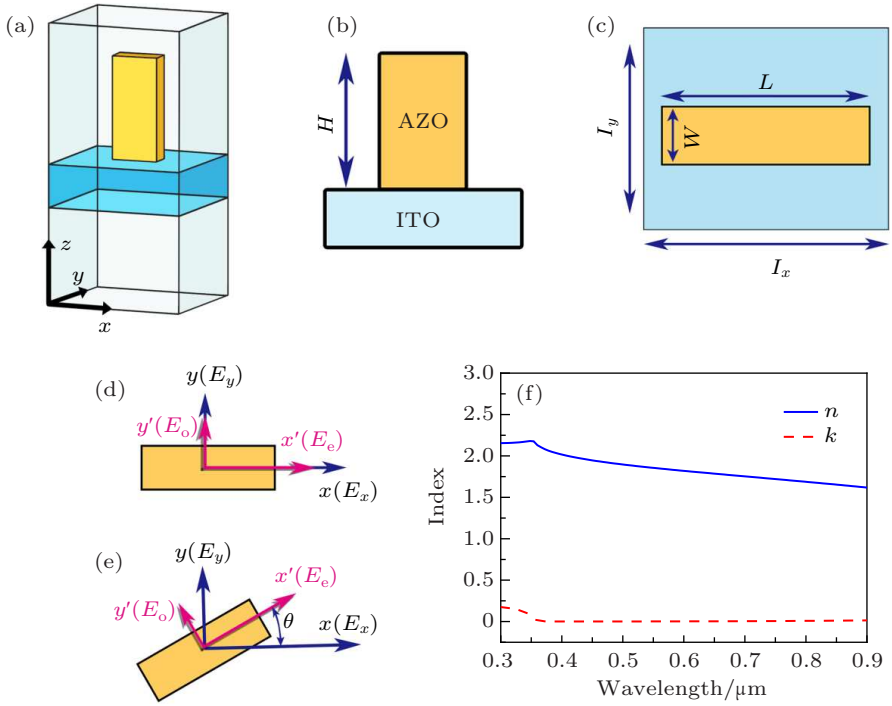


**Fig. 1.** (a) Structure of the AZO unit cell. (b) The longitudinal cross-section of the AZO unit cell with a height of $H$. (c) The transverse section of the AZO unit cell, where $L$ and $W$ represent the length and width of AZO nanorod, and $I_x$, $I_y$ represent the length and width of ITO substrate. (d) Crystal axes (fast axis and low axis) coincide with $E_x$ and $E_y$ of the incident wave. (e) The AZO nanorod rotated by $\theta$. (f) AZO refractive index $n,k$ diagram.

## 3. Results and discussion

The maximum polarization conversion efficiency and the corresponding wavelength position can be regulated by adjusting the structural parameters. Figure 2 shows the polarization conversion efficiency curves of three different structures, and the specific parameters are shown in Table 1. The high conversion efficiency indicates that it is very suitable for use in applications, such as half-wave plates. Even for the S3 structure, the narrow-wave region at 372 nm also has a higher conversion efficiency of 78.86% due to the phase difference of 540°, which can be inferred from Fig. 4(f), so structure S3 also has a half-wave effect. The results of the polarization conversion rates for the three structures (S1–S3) exhibit that the AZO with higher height corresponds to the larger redshift of wavelength, meaning that the wavelength of the peak polarization conversion efficiency can be effectively changed by adjusting the $H$ value. Usually the AZO material with a wide bandgap has one strong absorption in ultraviolet (around 378 nm), it is not suitable to be used as a half-wave plate in the UV region due to strong absorption. This is contrary to the above results.

**Table 1.** Structure parameters of S1, S2, and S3.

| Structure | S1 | S2 | S3 |
|---|---|---|---|
| Length ($L$)/nm | 45 | 45 | 45 |
| Width ($W$)/nm | 90 | 90 | 90 |
| Height ($H$)/nm | 1400 | 1850 | 2600 |
| $I_x$/nm | 100 | 100 | 100 |
| $I_y$/nm | 100 | 100 | 100 |

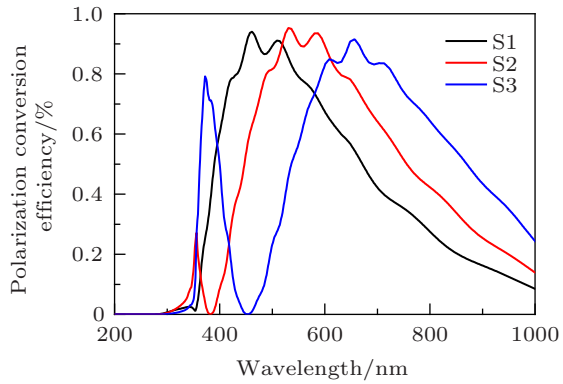


**Fig. 2.** Polarization efficiency of the three structures, the incident light with left/right circled polarization and the transmission light with right/light circled polarization.

The dependences of the polarization conversion efficiency and peak position on the AZO plate's width $W$ and length $L$, substrate's length $I_x$ and width $I$ are investigated, as shown in Fig. 3. It can be seen that one individual of the $W$, $I_x$, and $I_y$ increases, or $L$ decreases, the polarization conversion efficiency will increase, while the peak position will blueshift or redshift. It shows that the increase of the ratio of length to width and the duty cycle will increase the efficiency of polarization conversion and make the peak blueshift. Furthermore, as shown in Fig. 2, the increase of $H$ makes the peak redshift. It can be inferred that the increase of efficiency is directly related to the ratio of length to width and the duty cycle of meta-atoms. Red-shifting and blue-shifting may be caused by the change of the phase of $E_x$ and $E_y$ after modulating parameters.

Birefringence occurs when an optical wave incident into an inhomogeneous medium, except for a special direction. The incident light is decomposed into two kinds of polarized light, they are perpendicular to each other in the direction of vibration with different propagation speeds and different refractive indexes.[22] As is known, circularly polarized light can be decomposed into two linearly polarized light along the $x$ axis ($E_x$) and along the $y$ axis ($E_y$). With the incident light irradiating on the AZO nanorod at $\theta = 0$, the birefringence phenomenon will occur, leading to the difference of phase between $E_x$ and $E_y$, as shown in Fig. 1(d) When the phase difference is odd times of 180°, the polarity of the circularly polarized light will be reversed.[23,24]

When the right/left polarization light is incoming along the $z$ axis to an AZO nanorod which has a rotation angle $\theta$, the right/left polarized light will conversion to left/right polarized light, and phase decreases/increases by $2\theta$. While at $\theta \neq 0$ (Fig. 4(a)), owing to the special structure of the AZO nanorod, the geometric phase of the transmitted reversing circularly polarized light will double the $\theta$, so the transmitted beam will add an additional $2\theta$ geometric phase. The $x'$ axis and $y'$ axis coincide with the fast axis and slow axis, with the angle $\theta$ different from the $xy$ coordinate system. If the incoming light is circularly polarized, the $E_{\text{out}}$ leaving the half-wave plate can be written as

$$E_{\text{out}} = T(\theta)\begin{bmatrix}1\\ \pm \mathrm{i}\end{bmatrix} = \mathrm{e}^{\pm \mathrm{i}2\theta}\begin{bmatrix}1\\ \mp \mathrm{i}\end{bmatrix}, \tag{1}$$

$$T(\theta) = \begin{bmatrix}\cos 2\theta & \sin 2\theta\\ -\sin 2\theta & -\cos 2\theta\end{bmatrix}. \tag{2}$$

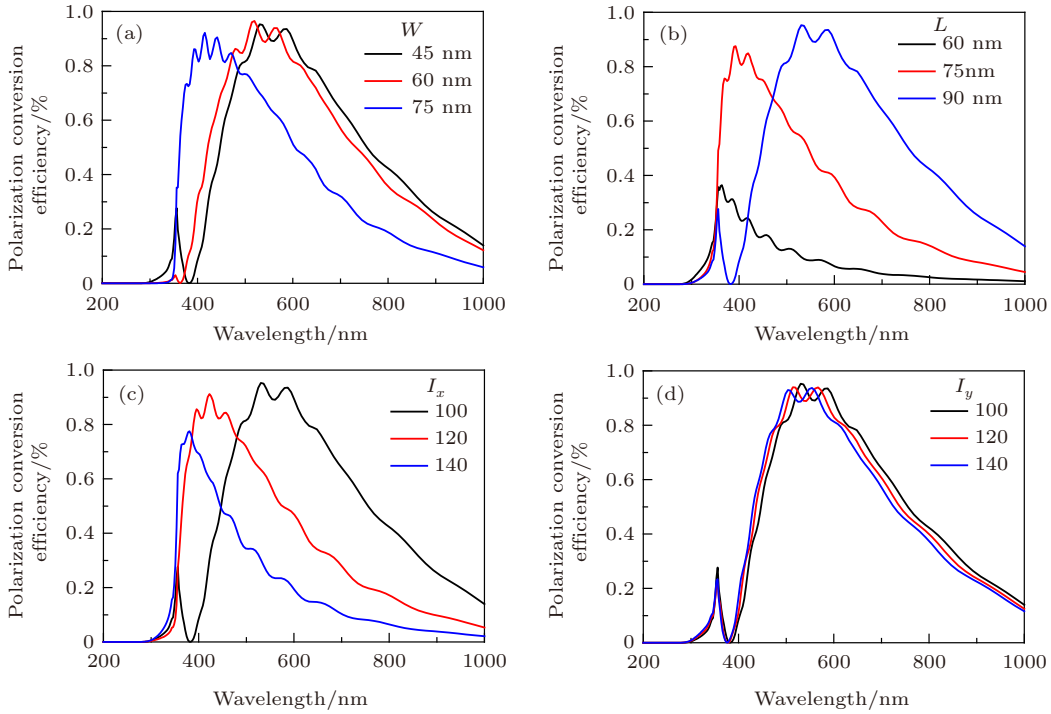


**Fig. 3.** Polarization conversion efficiency versus wavelength for different AZO plates: (a) AZO plates with different width $W$; (b) AZO plates with different length $L$; (c), (d) substrates with different length $I_x$ and width $I_y$, respectively.

Here $T(\theta)$ is the Jones matrix expression of a half-wave plate. It can be seen that the action of the half-wave plate can reverse the direction of circular polarization, and attach a $2\theta$ phase factor. If the $\theta$ changes from 0 to $\pi$, the change of phase will be from 0 to $2\pi$, which covers all angles. To prove the correctness of the derivation above and compare the difference between simulation and theory, we do the following test: rotate the AZO nanorod by $\theta$ around the $z$ axis to see the difference of the $\psi$ phase between theory and simulation. From Fig. 4, we can see that the theory and simulation results are very close, indirectly proving the correctness of the theory.

A 1-D design is corresponding to the schematic in Fig. 5(a), where $f$ is the focal length, $x$ is the transverse distance of a single AZO nanorod to the center of the metalens, and $\theta$ is the rotation angle between the $x$ axis and the fast axis. To take advantage of the properties of the above half-wave plates, we design metalens using the PB phase method. Because the phase retardation will inevitably lead to the optical path difference, which will make a wave-front change,[25–27] we design the $\theta$ of the structure by changing the length of the AZO coordinate away from the center position, which can theoretically realize the metalens. Its basic design principle[28,29] is

$$\theta = \frac{\pi}{\lambda}\left(\sqrt{f^2+x^2}-f\right). \tag{3}$$

The 1-D structure can be extended to 2-D,[30] as shown in Figs. 5(b) and 5(c). For the 2-D AZO unit cells, we have

$$\theta = \frac{\pi}{\lambda}\left(\sqrt{f^2+x^2+y^2}-f\right). \tag{4}$$

And the additional geometric phase is

$$\phi = \frac{2\pi}{\lambda}\left(\sqrt{f^2+x^2+y^2}-f\right) = 2\theta. \tag{5}$$

Figures 6(a)–6(c) show that the phase shift has a remarkable change at the polarization direction along $x$, the difference between the two incident light is close to $\pi$ at the corresponding wavelength with $z = 4$ μm, detailed data are available in Table 2. For example, when the 450 nm light is leaving the AZO nanorod, the phase retardation of $E_x$ between the structures with and without the AZO is $2.552\pi$, $E_y$ is $1.356\pi$, and the phase retardation between $E_x$ and $E_y$ is $1.196\pi$. The rest is the same. The dashed lines in Figs. 6(d)–6(f) show that the wavelength corresponding to the phase difference $\pi$ is approaching to the wavelength with respect to the maximum polarity conversion efficiency of the half-wave plate, indicating that the simulation is in good agreement with the theory.

**Table 2.** Phase shift of $E_x$ and $E_y$ for linearly polarized incident light at 450 nm, 530 nm, and 650 nm with respect to Figs. 6(d)–6(f).

| Wavelength | 450 | 530 | 650 |
|---|---|---|---|
| $E_x$ (with structure)/$\pi$ | 20.321 | 17.601 | 14.939 |
| $E_x$ and $E_y$ (without structure)/$\pi$ | 17.769 | 15.053 | 12.304 |
| $E_y$ (with structure)/$\pi$ | 19.125 | 16.446 | 13.802 |
| Phase shift of $E_x$/$\pi$ | 2.552 | 2.548 | 2.635 |
| Phase shift of $E_y$/$\pi$ | 1.356 | 1.393 | 1.498 |
| Phase difference/$\pi$ | 1.196 | 1.155 | 1.137 |

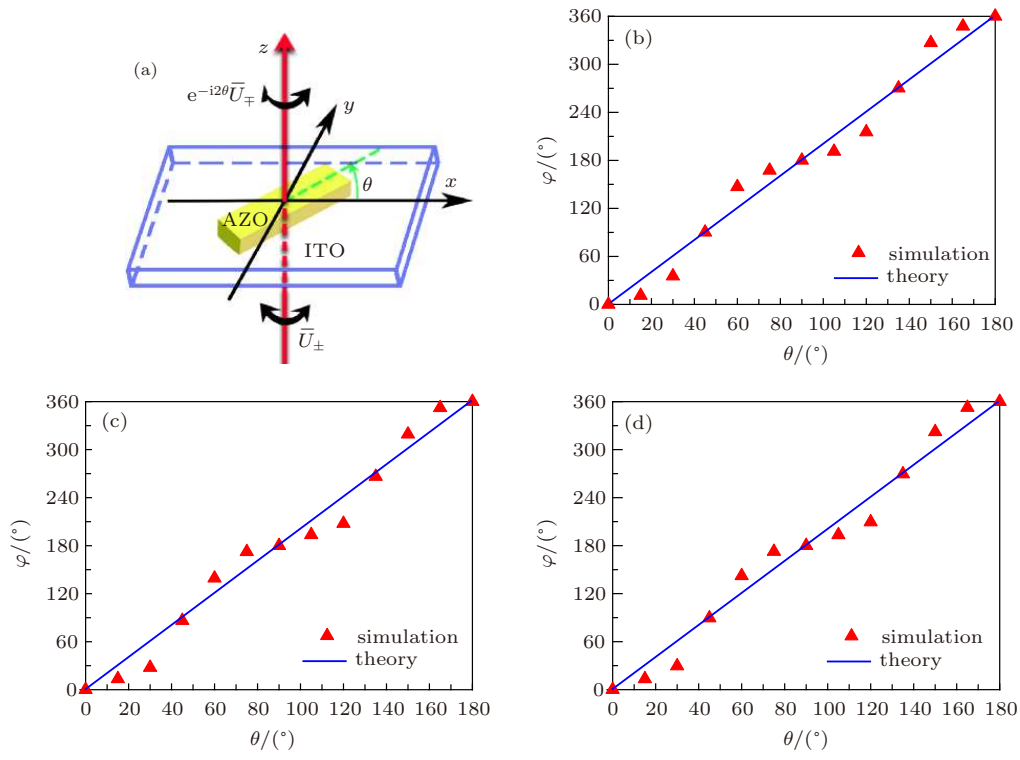


**Fig. 4.** (a) Schematic of polarity flip. (b)–(d) The relationship between the additional phase $\varphi$ of the transmission field and the $\theta$ angle for samples S1 (450 nm), S2 (530 nm), and S3 (650 nm), respectively.

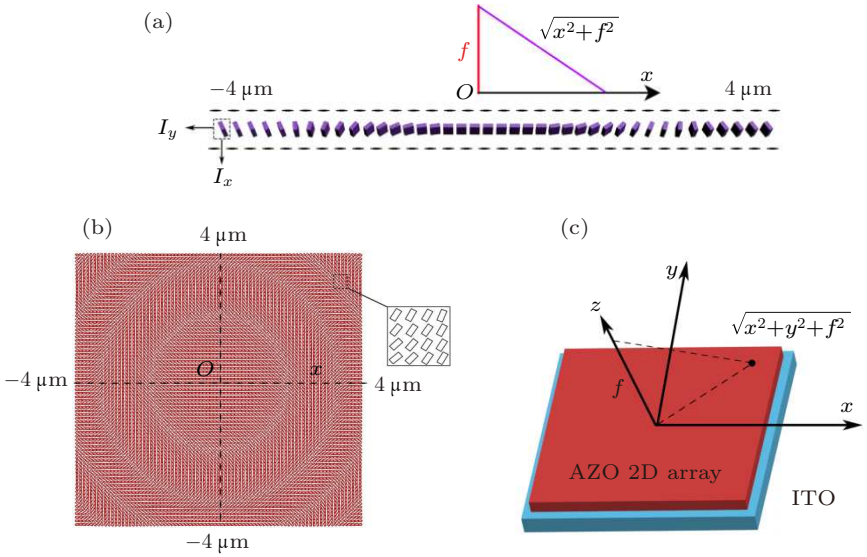


**Fig. 5.** Schematic of metalens designed according to PB phase method: (a) 1-D metalens, (b), (c) 2-D metalens.

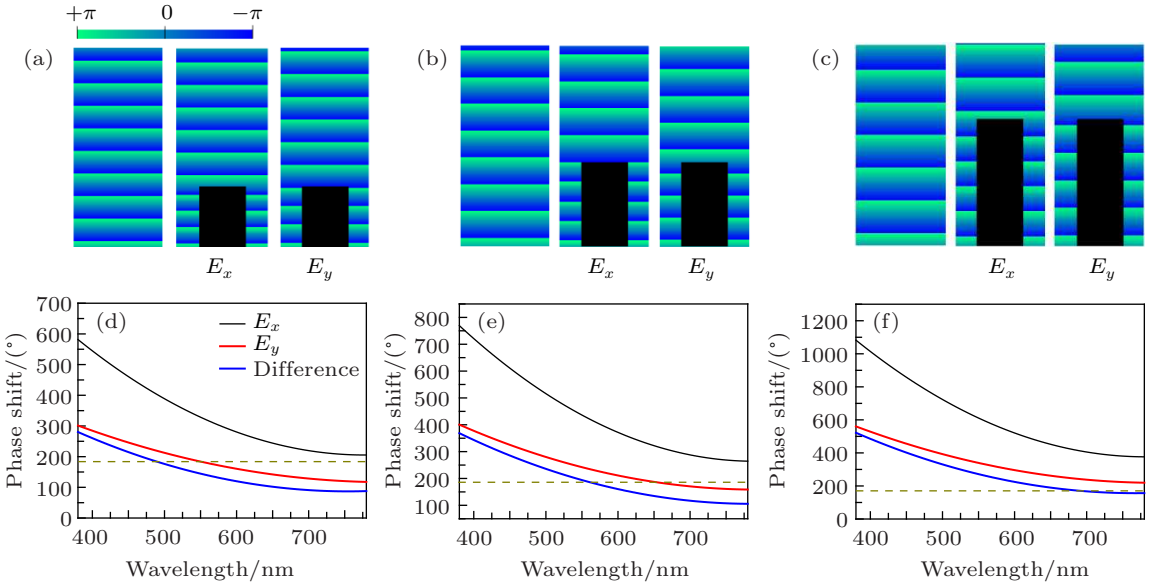


**Fig. 6.** The phase profiles of $E_x$ and $E_y$ for the three structures: (a) S1 (450 nm), (b) S2 (530 nm), (c) S3 (650 nm), where the left picture in (a)–(c) is corresponding to the one without AZO. At $z = 4$ μm, the retardation phase curves of $E_x$, $E_y$ and their differences for (d) S1 (450 nm), (e) S2 (530 nm), (f) S3 (650 nm).

Figure 7 displays the intensity distribution and phase cross section of the 1-D metalens designed with Eq. (3), the transverse span ($x$ span) is 20 μm, the incident light is the circular polarization light. When light is transmitted from the lens, the original planar wave will be converted into a circular planar wave,[31] and due to the phase differences between $E_o$ and $E_e$, the wave-front plane will form a cone plane, which can be observed from the intensity distribution, as shown in Figs. 7(a)–7(c). The phase profile diagram also exhibits the same results, as shown in Figs. 7(g)–7(i) and the focus center is located at $z = 10$ μm. Meanwhile, it is observed from Figs. 7(d)–7(f), the 2-D metalens (Figs. 5(b) and 5(c)) with a rectangular range of 8 μm×8 μm will be more suitable. The three kinds of metalens combined with three kinds of structures are all regularly arranged $80 \times 80$ AZO nanorods.

The intensity distribution of $x$–$z$ section of 2-D metalens can be seen from Figs. 8(a)–8(c). We can see that the focus effect is very well. Especially, one can find that there are two focuses at point 1 and point 2, where point 1 represents the stronger one. The presented bifocuses were rarely reported before. The $z$ value, intensity distribution, $x$–$y$ normalized intensity, full width at half-maximum (FWHM), and focus size (the full width at 90% maximum) of each focal spot are shown in Figs. 8 and 9. The intensities corresponding to different $z$ values in the $x$–$y$ plane are shown in Figs. 8(d)–8(i). It shows that the focal length and focal size of the three kinds of structures are different, but they change regularly. In other word, with the increase of the $H$ value of the meta-atoms, the focal length of the metalens (light intensity) decreases and the focal size increases, which are the results of phase modulation.

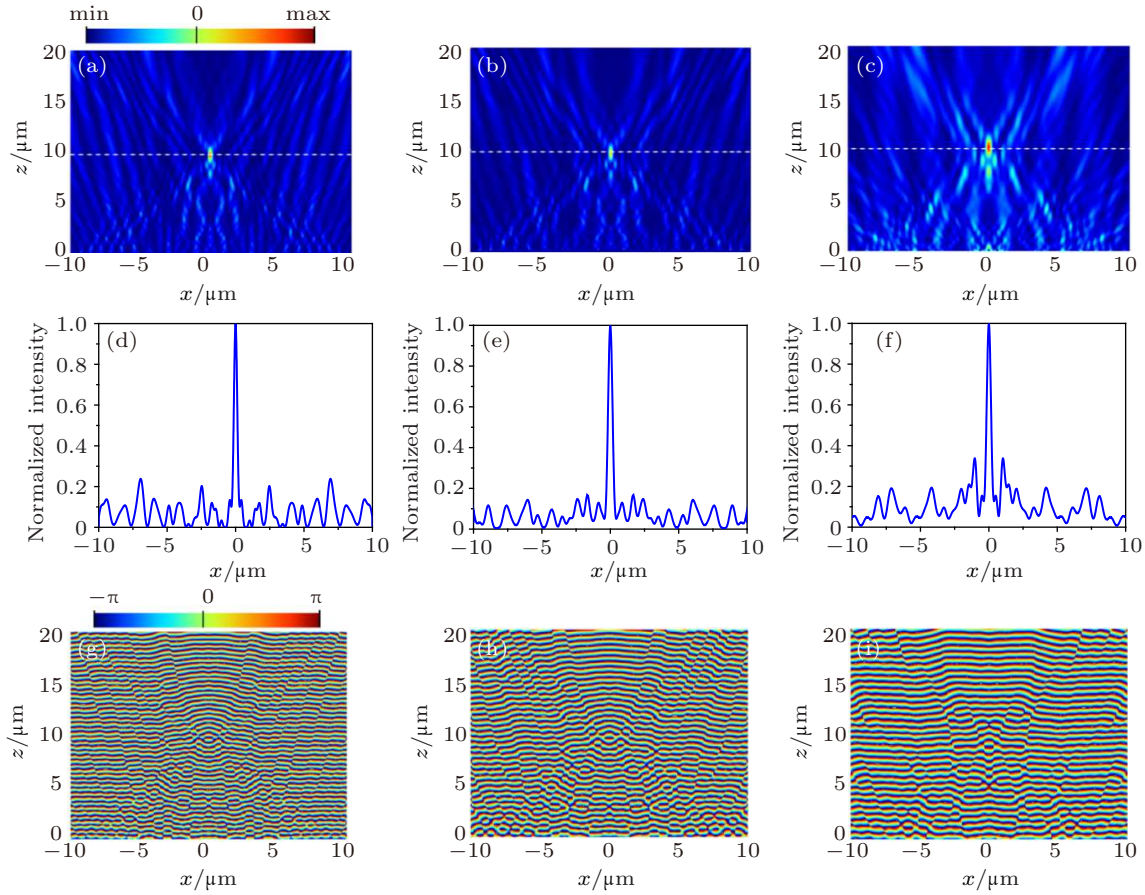


**Fig. 7.** The 1-D AZO metalens designed based on Fig. 3(a) with a total transverse length of 20 μm, with a circularly polarized incident light. (a)–(c) The diagram of power distribution in the $x$–$z$ plane for the S1 (450 nm), S2 (530 nm), and S3 (650 nm), respectively. (d)–(f) Normalized intensity diagrams based on the three images at $z = 10$ μm. (g)–(i) $x$–$z$ plane phase profile diagram at $y = 0$ μm in the $x$–$z$ plane.

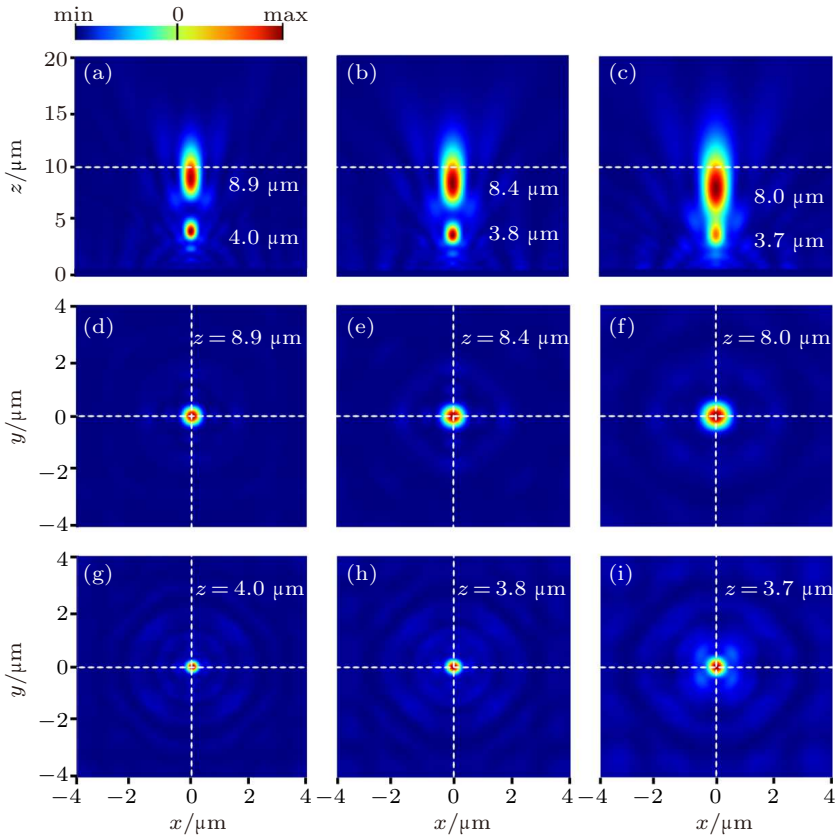


**Fig. 8.** The intensity distribution on $x$–$z$ plane of 2-D metalens: (a) S1 (450 nm), (b) S2 (530 nm), (c) S3 (650 nm), the $z$ coordinates of two focal points are marked on the graph. (d)–(i) The $x$–$y$ section of intensity distribution diagram at corresponding $z$ values (marked in the upper right corner).

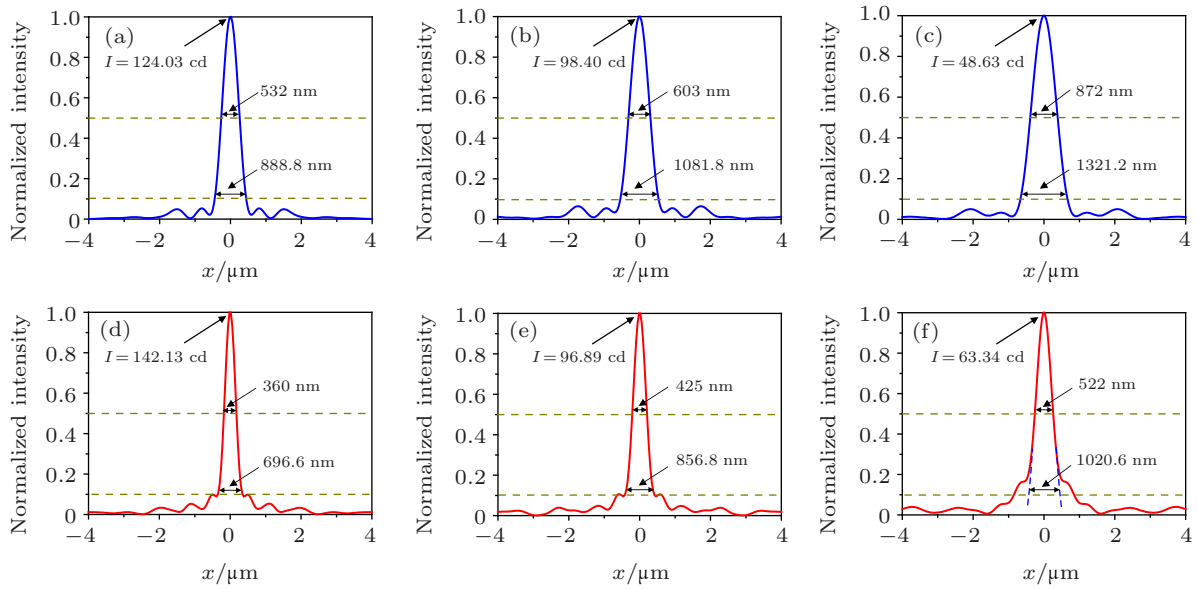


**Fig. 9.** (a)–(f) The normalized intensity diagram on the $x$-$y$ plane at different $z$ values corresponding to the six focal points in Figs. 8(d)–8(i).

In order to further study the reason of the bifocuses, we modulate the total number of single AZO unit cells (Fig. 10) and find that if the array is $60 \times 60$ (Fig. 10(a)) or $40 \times 40$ (Fig. 10(b)), no bifocuses are observed. Therefore, the existence of bifocus is due to the modulation of the optical wavefront by the peripheral array of AZO nanorods. At the same time, we find that increasing the number of peripheral AZO nanorods will make the focal length close to the set value (10 μm), which can be inferred from Figs. 10 and 8(b). We can define the ratio of the power contained in a circle with the diameter of the triple of the half peak width (FWHM) to the total power of the light source to calculate the focusing efficiency of each focus point, the corresponding focusing efficiency is shown in Table 3. It is noted that the focusing efficiency of point 1 is 53.6%, 60.6%, and 64.5% for the three kinds of metalens with the S1, S2, and S3 structures, respectively. In addition, note that the numerical aperture (NA)[32] of point 2 is relatively large (Table 3), which is only in a vacuum ($N = 1$). If oil[33] or other liquid with a high refractive index is added between the metalens and the focal plane, the numerical aperture can be larger than 1 and is very large. And the emergence of a negative index of refraction or strongly anisotropic materials will break the theoretical bottleneck of traditional resolution.[34] Furthermore, the coverage of polarity conversion of single mechanism cells is narrow, it may not be effective to eliminate the effect of color aberration on imaging. Thus, this work needs further improvement.

**Table 3.** Focusing efficiency (FE) and NA of 2D-metalen with structures (S1, S2, S3) designed by PB phase method.

| Structure | FE of point 1 | FE of point 2 | NA of point 1 | NA of point 2 |
|---|---|---|---|---|
| S1 | 0.536 | 0.238 | 0.410 | 0.707 |
| S2 | 0.606 | 0.273 | 0.430 | 0.725 |
| S3 | 0.645 | 0.337 | 0.447 | 0.721 |

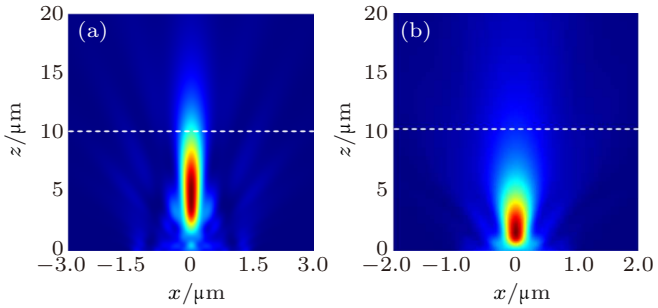


**Fig. 10.** The $x$–$z$ cross-section intensity distribution of 2D-metalens with the S3 structure of AZO nanorods by the PB phase method: (a) $60 \times 60$ AZO nanorods, (b) $40 \times 40$ AZO nanorods.

## 4. Conclusion

Three types of AZO-based half-waves plates in the visible light band have been designed based on half-wave theory, where the half-wave polarization conversion efficiency of the unit cell reaches as high as 91.48%. Based on this, we design 1-D and 2-D metalens, which can be used for focusing under visible light. Software simulation is used to prove the feasibility of the construction. When the metalens are regularly arranged with a suitable number of AZO nanorods (for example $80 \times 80$ array), bifocus with a high focusing efficiency can be observed. At the same time, we compare the phase simulation with the theory, and the simulation results are in good agreement with the theoretical values.

As for the fabrication strategy of this device, one can prepare the AZO film on ITO substrate with magnetron sputtering, then design mask according to the AZO nanorod arrays as displayed in Fig. 5, and etch down the AZO film with Si as the mask to obtain AZO metalens using semiconducting fabrication process. In principle, we can obtain the designed AZO metalens, the main obstacle is the extremely high aspect ratio. In the experiment, we can increase the aspect ratio gradually

to the desired value. We hope that the design of the metalens will enrich the application of nanophotonics and the metalens can be used effectively.

For the final devices, many efforts are needed. Our designed metalens will be useful for the practical development of low loss devices in the visible range, which can be applied to half-wave conversion, imaging, photovoltaic printing, phase and amplitude modulation, and so on.

## Acknowledgment

We thank Dr. Zhengchang Liu from Peking University for his instructional assistance.

## References

[1] Liu Z, Lee H, Xiong Y, Sun C and Zhang X 2007 *Science* **315** 1686
[2] Smolyaninov I I, Hung Y J and Davis C C 2007 *Science* **315** 1699
[3] Khorasaninejad M, Chen W T, Devlin R C, Oh J, Zhu A Y and Capasso F 2016 *Science* **352** 1190
[4] Ye M, Ray V and Yi Y 2018 *IEEE Photonics Technology Lett.* **30** 955
[5] Xu H, Tang S, Sun C, Li L, Liu H, Yang X, Yuan F and Sun Y 2018 *Photonics Research* **6** 782
[6] Li L, Zhang X, Song C and Huang Y 2020 *Appl. Phys. Lett.* **116** 060501
[7] Zhang J, Tian Y, Cheng Y and Liu X 2020 *Appl. Phys. Lett.* **116** 030501
[8] Fehrenbacher M, Winnerl S, Schneider H, Doring J, Kehr S C, Eng L M, Huo Y, Schmidt O G, Yao K, Liu Y and Helm M 2015 *Nano Lett.* **15** 1057
[9] Guo L, Xu S, Wan R, Li T, Xiong L, Wang L and Zhu W 2018 *J. Nanophoton.* **12** 1
[10] Chen B H, Wu P C, Su V C, Lai Y C, Chu C H, Lee I C, Chen J W, Chen Y H, Lan Y C and Kuan C H 2017 *Nano Lett.* **17** 6345.
[11] Kelly P, Liu M and Kuznetsova L 2016 *Appl. Opt.* **55** 2993
[12] Masouleh F F, Sinno I, Buckley R G, Gouws G and Moore C P 2018 *Appl. Phys. A* **124** 178
[13] Li X, Jiao L, Xu H, Lu Y, Zhu C, Duan J, Zhang X, Dai N and Song W 2016 *Optical Materials Express* **6** 3892
[14] Pepe Y, Yildirim M A, Karatay A, Ates A, Unver H and Elmali A 2019 *Optical Materials* **98** 109495
[15] Shah A, Ahmad M, Rahmanuddin, Khan S, Aziz U, Ali Z, Khan A and Mahmood A 2019 *Appl. Phys. A* **125** 713
[16] Hakan Karaagac E Y and Islam M S 2012 *J. Alloys Compd.* **51** 155
[17] Naik G V, Liu J, Kildishev A V, Shalaev V M and Boltasseva A 2011 *Appl. Phys. B* **103** 553
[18] Berry M V 1987 *J. Modern Opt.* **34** 1401
[19] Xu H X, Liu H, Ling X, Sun Y and Yuan F 2017 *IEEE Trans. Antennas Propaga.* **65** 7378
[20] Zhang J L, Lan X, Zhang C, Liu X Y and He F T 2020 *Optik* **204** 163852
[21] Kargar R, Rouhi K and Abdolali A 2020 *Opt. Commun.* **462** 125331
[22] An G, Li S, Yan X, Yuan Z and Zhang X 2016 *Appl. Opt.* **55** 1262
[23] Guo L, Hu Z, Wan R, Long L, Li T, Yan J, Lin Y, Zhang L, Zhu W and Wang L 2018 *Nanophotonics* **7** 1651
[24] Liu Z, Li Z, Liu Z, Cheng H, Liu W, Tang C, Gu C, Li J, Chen H T and Chen S 2017 *ACS Photonics* **4** 2061
[25] Wang W, Guo C, Zhao Z, Li J and Shi Y 2020 *Results in Physics* **17** 103033
[26] Xu H.X, Hu G, Li Y, Han L, Zhao J, Sun Y, *et al.* 2019 *Light Sci. Appl.* **8** 3
[27] Xu H, Han L, Li Y, Sun Y, Zhao J, Zhang S and Qiu C 2019 *ACS Photonics* **6** 211
[28] Khorasaninejad M and Capasso F2017 *Science* **358** eaam8100
[29] Chen W T, Zhu A Y, Sanjeev V, Khorasaninejad M, Shi Z, Lee E and Capasso F 2018 *Nat. Nanotechnol.* **13** 220
[30] Yang Q, Gu J, Xu Y, Zhang X, Li Y, Ouyang C, Tian Z, Han J and Zhang W 2017 *Adv. Opt. Mater.* **5** 1601084
[31] Aieta F, Genevet P, Kats M and Capasso F 2013 *Opt. Express* **21** 31530
[32] Liang H, Lin Q, Xie X, Sun Q, Wang Y, Zhou L, Liu L, Yu X, Zhou J, Krauss T F and Li J 2018 *Nano Lett.* **18** 4460
[33] Chen W T, Zhu A Y, Khorasaninejad M, Shi Z, Sanjeev V and Capasso F 2017 *Nano Lett.* **17** 3188
[34] Lu D and Liu Z 2012 *Nat. Commun.* **3** 1160